The evolution of quiescent galaxies at high redshifts (z≥ 1.4)

Monthly Notices
of the
ROYAL ASTRONOMICAL SOCIETY

Mon. Not. R. Astron. Soc. **417,** 900–915 (2011) doi:10.1111/j.1365-2966.2011.19263.x

The evolution of quiescent galaxies at high redshifts ($z \geq 1.4$)

H. Domínguez Sánchez,[1,2]★ F. Pozzi,[3] C. Gruppioni,[1] A. Cimatti,[3] O. Ilbert,[4] L. Pozzetti,[1] H. McCracken,[5] P. Capak,[6,7] E. Le Floch,[8] M. Salvato,[9] G. Zamorani,[1] C. M. Carollo,[10] T. Contini,[11] J.-P. Kneib,[12] O. Le Fèvre,[12] S. J. Lilly,[10] V. Mainieri,[13] A. Renzini,[14] M. Scodeggio,[15] S. Bardelli,[1] M. Bolzonella,[1] A. Bongiorno,[16] K. Caputi,[10,17] G. Coppa,[1,3] O. Cucciati,[18] S. de la Torre,[15,19] L. de Ravel,[12,17] P. Franzetti,[15] B. Garilli,[15] A. Iovino,[19] P. Kampczyk,[10] C. Knobel,[10] K. Kovač,[10] F. Lamareille,[11] J.-F. Le Borgne,[11] V. Le Brun,[12] C. Maier,[10] M. Mignoli,[1] R. Pelló,[11] Y. Peng,[10] E. Perez-Montero,[11,20] E. Ricciardelli,[2,14] J. D. Silverman,[10,21] M. Tanaka,[13,21] L. A. M. Tasca,[12,15] L. Tresse,[12] D. Vergani[1] and E. Zucca[1]

[1]*INAF-Osservatorio Astronomico di Bologna, via Ranzani 1, I-40127 Bologna, Italy*
[2]*Instituto de Astrofísica de Canarias, 38205 La Laguna, Spain*
[3]*Alma Mater Studiorum Università di Bologna, Dipartimento di Astronomia, via Ranzani 1, I-40127 Bologna, Italy*
[4] *Laboratoire d'astrophysic de Marseille, Universitè de provence, CNRS, BP 8, Traverse du Siphon, 13376 Marseille Cedex 12, France*
[5] *Institute d'astrophysic de Paris, UMR7095 CNRS, Universitè Pierre et Marie Curie, 98 bis Boulevard Arago, 75014 Paris, France*
[6]*Spitzer Science Center, 314-6 Caltech, Pasadena, CA 91125, USA*
[7]*Department of Astronomy, 249-17 Caltech, Pasadena, CA 91125, USA*
[8]*Laboratoire AIM, CEA/DSM-CNRS-Universite Paris Diderot, IRFU/Service d'Astrophysique, CEA-Saclay, 91191 Gif-sur-Yvette Cedex, France*
[9]*Max Planck Institute for Plasma Physics and Excellence Cluster Universe, Boltzmannstr. 2 D-85748 Garching, Germany*
[10]*ETH Zurich, Institute of Astronomy, Wolfgang-Pauli-Straße 27, 8093 Zurich, Switzerland*
[11]*Laboratoire d'Astrophysique de Toulouse-Tarbes, Université de Toulouse, CNRS, 14 avenue Edouard Belin, 31400 Toulouse, France*
[12]*Laboratoire d'Astrophysique de Marseille, Université d'Aix-Marseille, CNRS, 38 rue Frédéric Joliot-Curie, 13388 Marseille Cedex 13, France*
[13]*European Southern Observatory, Karl-Schwarzschild-Straße 2, 85748 Garching bei München, Germany*
[14]*INAF - Osservatorio Astronomico di Padova, vicolo dell'Osservatorio 5, 35122 Padova, Italy*
[15]*INAF - IASF Milano, via Bassini 15, 20133 Milano, Italy*
[16]*Max-Planck-Institut für Extraterrestrische Physik, Giessenbachstraße, 84571 Garching bei München, Germany*
[17]*Institute for Astronomy, Royal Observatory, Blackford Hill, Edinburgh EH9 3HJ*
[18]*INAF - Osservatorio Astronomico di Trieste, via G. B. Tiepolo 11, 34143 Trieste, Italy*
[19]*INAF - Osservatorio Astronomico di Brera, via Brera 28, 20121 Milano, Italy*
[20]*Instituto de Astrofisica de Andalucia, CSIC, Apdo. 3004, 18080 Granada, Spain*
[21]*Institute for the Physics and Mathematics of the Universe (IPMU), University of Tokyo, Kashiwanoha 5-1-5, Kashiwa-shi, Chiba 277-8568, Japan*

Accepted 2011 June 15. Received 2011 June 15; in original form 2011 March 30

ABSTRACT

The goal of this work is to study the evolution of high-redshift ($z \geq 1.4$) quiescent galaxies over an effective area of $\sim$1.7 deg^2 in the COSMOS field. Galaxies have been divided according to their star formation activity and the evolution of the different populations, in particular of the quiescent galaxies, has been investigated in detail. We have studied an IRAC ($\mathrm{mag}_{3.6\,\mu\mathrm{m}} < 22.0$) selected sample of $\sim$18 000 galaxies at $z \geq 1.4$ in the COSMOS field with multiwavelength coverage extending from the *U* band to the *Spitzer* 24 μm one. We have derived accurate photometric redshifts ($\sigma_{\Delta z/(1+z_s)} = 0.06$) through a SED-fitting procedure. Other important physical parameters [masses, ages and star formation rates (SFR)] of the galaxies have been obtained using Maraston models. We have divided our sample into actively star-forming, intermediate and quiescent galaxies depending on their specific star formation

★E-mail: helena.dominguez@oabo.inaf.it

rate (SSFR = SFR/M). We have computed the galaxy stellar mass function (GSMF) of the total sample and the different populations at $z = 1.4$–3.0. We have studied the properties of high-redshift quiescent galaxies finding that they are old (1–4 Gyr), massive ($\langle M \rangle \sim 10^{10.65}\,\mathrm{M}_{\odot}$), weakly star-forming stellar populations with low dust extinction [$E(B-V) \leq 0.15$] and small e-folding time-scales ($\tau \sim 0.1$–0.3 Gyr). We observe a significant evolution of the quiescent stellar mass function from $2.5 < z < 3.0$ to $1.4 < z < 1.6$, increasing by $\sim$1 dex in this redshift interval. We find that $z \sim 1.5$ is an epoch of transition of the GSMF: while the GSMF at $z \gtrsim 1.5$ is dominated by the star-forming galaxies at all stellar masses, at $z \lesssim 1.5$ the contribution to the total GSMF of the quiescent galaxies is significant and becomes higher than that of the star-forming population for $M \geq 10^{10.75}\,\mathrm{M}_{\odot}$. The fraction of star-forming galaxies decreases from 60–20 per cent from $z \sim 2.5$–3.0 to 1.4–1.6 for $M \sim 10^{11.0}\,\mathrm{M}_{\odot}$, while the quiescent population increases from 10–50 per cent at the same redshift and mass intervals. We compare the fraction of quiescent galaxies derived with that predicted by theoretical models and find that the Kitzbichler & White model, implemented on the Millennium Simulation, is the one that better reproduces the shape of the data. Finally, we calculate the stellar mass density of the star-forming and quiescent populations as a function of redshift and find that there is already a significant number of quiescent galaxies at $z > 2.5$ ($\log\rho\ [\mathrm{M}_{\odot}\,\mathrm{Mpc}^{-3}] \sim 6$), meaning that efficient star formation had to take place before that time.

Key words: galaxies: evolution – galaxies: high-redshift – galaxies: star formation.

1 INTRODUCTION

Understanding the processes that regulate stellar mass growth in galaxies as well as tracing the history of galaxy star formation and mass assembly over the cosmic time (Lilly et al. 1996; Madau et al. 1996; Pozzetti et al. 1998; Dickinson et al. 2003) are among the most important and discussed topics in modern cosmology. During the last decade, extraordinary progress has been made in our comprehension of the formation and evolution of galaxies. Thanks to deep multiwavelength surveys we are now able to observe large samples of distant galaxies, thus reducing cosmic variance and allowing us to study objects at early cosmic times.

In the present Universe, it is known that galaxies can be separated into two broad populations: passively evolving galaxies with red colours, also known as quiescent galaxies or early-type galaxies (ETGs hereafter), and star-forming galaxies with blue colours (e.g. Baldry et al. 2004; Brinchmann et al. 2004). A similar division extends to at least $z \sim 1$ (Bell et al. 2004; Willmer et al. 2006) and possibly to $z \sim 2$ (Giallongo et al. 2005; Cirasuolo, McLure & Dunlop 2007; Cassata et al. 2008).

ETGs are the most massive galaxies in the present day Universe and are characterized by simple and homogeneous properties (morphologies, colours, passively evolving stellar populations, scaling relations). As a consequence, they are a key population to investigate the stellar mass assembly of massive galaxies over the cosmic time (e.g. Renzini 2006). Gallazzi et al. (2006) studied the properties of local quiescent galaxies and, in particular, the colour–magnitude and the Mg_2–σ_{v} relation. They found that for high-mass elliptical galaxies the dispersion in age is small, while at the low mass end there is a tail towards younger ages, reflecting a shift in stellar growth towards less massive galaxies in recent epochs. Besides, they also argue that at increasing stellar mass there is also an increase in both total metallicity and α/Fe ratio, suggesting that massive early type galaxies formed in a relatively short time-scale. The stellar mass and ages of the passive ETGs at $z \sim 1$–2 require precursors characterized by strong ($>100\,\mathrm{M}_{\odot}\,\mathrm{yr}^{-1}$) and short-lived (0.1–0.3 Gyr) starbursts occurring at $z > 2$–3 (e.g. Cimatti 2009 and references therein).

Stellar mass assembly in galaxies subdivided by spectral and morphological types, as well as by star formation activity has been investigated at $z > 0$ by many authors (e.g. Bundy et al. 2005; Franceschini et al. 2006; Pannella et al. 2006; Pozzetti et al. 2010). Cimatti (2006) studied the B-band luminosity function of ETGs since $z \sim 1$, finding that the amount of the evolution for the ETG population depends critically on the range of masses considered, i.e. most of the massive ETGs are already in place at $z \sim 1$, while the density is still increasing with time for lower masses. This means that more massive galaxies have older stellar populations and formed their stars earlier and more rapidly than low-mass galaxies, in agreement with Gallazzi et al. (2006). Therefore, the downsizing pattern (Cowie et al. 1996) could be applied to the assembly process of ellipticals at $z < 1$. The downsizing trend is also confirmed by a recent work based on a spectroscopic sample up to $z \sim 1$ in the COSMOS field (Pozzetti et al. 2010) that showed how the ETGs increase in number density with cosmic time faster for decreasing M. They also found that the number density of blue or spiral galaxies with $M > 10^{10}\,\mathrm{M}_{\odot}$ remains almost constant, while the most extreme population of star-forming galaxies at intermediate/high mass is rapidly decreasing in number density with cosmic time. The authors suggest a transformation from blue active spiral galaxies of intermediate mass into blue quiescent and successively into red passive types with low specific star formation. This is in agreement with the result obtained by Faber et al. (2007) who concluded that most present-day E/S0 near L^* arose from blue galaxies with ongoing star formation that were quenched after $z \sim 1$ and then migrated to the red sequence. The properties of nearby ETGs support a mixed scenario in which quenched galaxies enter the red sequence via wet, gas-rich mergers, followed by a limited number of dry, stellar mergers along the sequence. The evolution of the stellar mass function of the ETGs up to $z \sim 1$ has also been studied by other authors (e.g. Bell et al. 2004; Brown et al. 2007; Nichol et al. 2007; Taylor et al. 2009), finding a moderate increase in the

number density of quiescent galaxies with cosmic time which is mass dependent.

At higher redshifts Arnouts et al. (2007) and Cirasuolo et al. (2007) found a rapid rise in the space density of massive red sequence galaxies from $z \sim 2$ to 1. These results are confirmed by Ilbert et al. (2010) who found that the stellar mass density of quiescent galaxies of all masses increases by 1.1 dex between $z \sim 1.7$ and 1, while it evolves only by 0.3 dex between 0.8–1 and $z \sim 0.1$. This trend is also confirmed by Fontana et al. (2009), who found that the fraction of quiescent galaxies increases from 15–20 per cent at $z > 2$ to ∼40 per cent at $z \sim 1.2$, and recently by Nicol et al. (2011), who found that the red sequence massive galaxies ($M > 10^{11}$ $M_{\odot}$) increase in mass density by a factor ∼4 from $z \sim 2$ to 1.

Some groups have claimed the existence of a population of massive galaxies at $z \sim 4$ (e.g. Mobasher et al. 2004; Yan et al. 2006; Rodighiero et al. 2007; Fontana et al. 2009; Mancini et al. 2009). The number density of these massive galaxies has had a substantial evolution between $z \sim 4$ and $z \sim 0$ (e.g. Marchesini et al. 2009, 2010, Caputi et al. 2011). Van Dokkum et al. (2010) derived that the present day 3×10^{11} $M_{\odot}$ galaxies have increased their stellar mass by a factor of ∼2 since $z \sim 2$ to the present. They concluded that this growth is likely dominated by mergers, as *in situ* star formation can only account for ∼20 per cent of the mass build up from $z = 2$ to 0.

Several studies suggest that the critical redshift range where the strongest evolution and assembly took place is $1 \leq z \leq 2$ (e.g. Abraham et al. 2007; Arnouts et al. 2007). However, while the results up to $z \sim 1$ are quite solid thanks to the large samples of galaxies and to the spectroscopic information available, the samples of ETGs studied up to now at $z > 1.4$ are still small. Besides, ETG are the more clustered galaxies in the Universe, making their study very complicated given field to field variations which introduce large uncertainties due to the cosmic variance. Anyway, many works have identified these objects spectroscopically, showing that passive/quiescent galaxies with elliptical morphology may exist up to $z \sim 2.5$ (Cimatti et al. 2004, 2008; McCarthy & GDDS 2004). There are even some candidates of ETGs at $z > 4$–5, but their nature is still unknown as they are optically too faint for being spectroscopically observed. Therefore, the uncertainties involved in the study of the evolution of quiescent galaxies at high redshifts are still large due to the observational difficulty to identify large samples of ETGs at high z (>1.5). In particular, long wavelength data are necessary to cover the optical–near-infrared (optical–NIR) part of the spectrum of high-redshift galaxies, a spectral range fundamental when calculating the galaxy stellar masses. In addition, the collection of a large sample of high-redshift galaxies requires a combination of large areas and deep NIR observations. Due to these difficulties, the study of the galaxy stellar mass function (GSMF hereafter) divided by galaxy types at $z > 1.5$ has been explored only roughly and our knowledge of the evolution of galaxies at high z is still rather poor.

Motivated by the limited information available at $z \geq 1.5$, we present in this paper the evolution of the GSMF with cosmic time at $z \geq 1.4$ for the total galaxy population and for the sample divided on the basis of the galaxy star-forming activity in the COSMOS field. The COSMOS survey is the perfect wide area sample to look for rare and clustered objects such as the old and massive ETGs with much improved statistics. This survey (Scoville et al. 2007) presents many advantages when compared with other surveys. First of all, the continuous coverage of $\sim 2\,\mathrm{deg}^2$ substantially reduces the effect of cosmic variance. Besides, its extensive multi-λ coverage allows to calculate accurate photometric redshifts (Ilbert et al. 2009) and to study the sources based on their spectral energy distributions (SEDs), which is a more physical and complete approach than using only colours or morphological information. Secondly, the multiwavelength data include deep *Spitzer*/IRAC (3.6–8.0 μm; Sanders et al. 2007) and K_s-band data (McCracken et al. 2010), crucial for estimating stellar masses at $z \sim 2$.

Galaxies of the present work are selected in the IRAC1 channel (3.6 μm), allowing to sample the optical–NIR stellar bump at $z > 1$. In addition, data at red wavelength are crucial to detect galaxies that are very faint in the optical (even undetected) but may contribute significantly to, or even dominate, the stellar mass density at high redshift (Yan 2000; Franx et al. 2003; Rodighiero et al. 2007). The extensive multiband data are used to separate galaxies into different populations based on their SEDs. The present work extends to higher redshifts the study of Ilbert et al. (2010). The sample of Ilbert et al. (2010) was selected at 3.6 μm as the present one, but their restriction to IRAC sources with an i^+-band counterpart ($i^+ < 25.5$) limited their study to $z \lesssim 2$ and to larger stellar masses. Our work was possible after a careful analysis of sources not detected in the optical.

The paper is organized as follows. In Section 2 we introduce the COSMOS data and the cross-correlation method. In Section 3 and 4 we describe the method to estimate the photometric redshifts and the galaxy stellar masses, while the criteria used to split the sample in different populations is described in Section 5. In Section 6 we study the main properties of the high-redshift quiescent galaxies and in Section 7 we present the GSMF for the whole sample and for the different populations, discussing our results in Section 8. Finally, in Section 9 we summarize our conclusions.

Throughout this paper we use standard cosmology ($\Omega_m = 0.3$, $\Omega_\Lambda = 0.7$), with $H_0 = 70\,\mathrm{km\,s^{-1}\,Mpc^{-1}}$. Magnitudes are given in AB system. The stellar masses are given in units of solar masses ($M_{\odot}$) for a Chabrier (Chabrier 2003) initial mass function (hereafter IMF). The stellar masses based on a Salpeter IMF were converted into a Chabrier IMF by adding −0.24 dex to the logarithm of stellar masses (Arnouts et al. 2007).

2 DATA

We have built a multiwavelength IRAC 3.6-μm selected catalogue in the COSMOS field by associating the IRAC sources with the optical and MIPS counterparts through the likelihood ratio method (see Section 2.2). For sources undetected at 5σ in the i^+-band selected catalogue we have performed a nearest match with the K_s-selected catalogue. The IRAC catalogue is 95 per cent complete at 5.75 μJy (22.0 mag). The final catalogue consists of 78 649 sources with $\mathrm{mag}_{3.6\,\mu m} < 22.0$: 95 per cent (74 742) of them with an optical counterpart, 4.5 per cent (3554) with no optical counterpart but a K_s-band counterpart and 0.5 per cent (353) with only IRAC detection. Besides, 14 per cent (11 352) of the IRAC sample are also detected in the MIPS band.

2.1 Catalogues

(i) *IRAC*. The COSMOS IRAC catalogue (Sanders et al. 2007) includes photometry in the four IRAC channels (3.6, 4.5, 5.8, 8.0 μm) for sources that have a measured flux in IRAC Channel 1 above 1 μJy (23.9 mag) in the COSMOS field. We used the 1.9 arcsec aperture corrected flux and we considered sources with $\mathrm{mag}_{3.6\,\mu m} < 22.0$.

(ii) *Optical*. The optical catalogue (Capak et al. 2007) is an i^+-band ($i < 26.5$ mag) selected catalogue in the area of the Subaru survey ($2\,\mathrm{deg}^2$) and includes photometry in nine bands

(u^*, B_J, g^+, V_J, r^+, i^+, z^+, J, K_s). We applied systematic offsets derived to optimize the photometric redshifts by Ilbert et al. (2009) and auto-offset corrections (which account for the aperture correction) to the optical catalogue.

(iii) *24 μm*. The 24-μm catalogue (Le Floc'h et al. 2009) is composed by sources detected above 0.15 mJy (18.5 mag).

(iv) K_s. The K_s-selected catalogue from McCracken et al. (2010) contains galaxies detected at K_s and additional data from B_J, i^+, z^+ and J bands. The catalogue is complete down to $K_s \sim 23$ mag. We applied a magnitude dependent aperture correction to the fluxes, as explained in McCracken et al. (2010).

2.2 The cross-correlation

We have performed a cross-correlation of the IRAC sources with the optical and MIPS catalogues through the likelihood ratio method.

The likelihood ratio technique (Sutherland & Saunders 1992; Ciliegi et al. 2003) has the advantage of taking into account not only the position (as for the nearest neighbour method, commonly used in literature), but also the magnitude distribution of the background sources, helping to reduce wrong identifications. The likelihood ratio LR is defined as the ratio between the probability that the source is the correct identification and the corresponding probability of a background, unrelated object:

$$LR = q(m) f(r)/n(m), \quad (1)$$

where $q(m)$ is the expected probability distribution, as a function of magnitude, of the true counterparts, $f(r)$ is the PDF of the positional errors of the IRAC sources (assumed to be a two-dimensional Gaussian) and $n(m)$ is the surface density of background objects with magnitude m. In order to derive an estimate for $q(m)$ we have first counted all objects in the optical/MIPS catalogue within a fixed radius around each source (total(m)). This has then been background subtracted and normalized to construct the distribution function of real identifications:

$$q(m) = \frac{\mathrm{real}(m) Q}{\sum_i \mathrm{real}(m)_i} \quad (2)$$

where $\mathrm{real}(m) = \mathrm{total}(m) - n(m)$ (the sum is over all the magnitude bins of the distribution) and Q is the probability that the optical/MIPS counterpart of the source is brighter than the magnitude limit of the optical/MIPS catalogue ($Q = \int^{m_{\rm lim}} q(m)\,\mathrm{d}m$). Finally, a best threshold value for LR ($\mathrm{LR_{th}}$) is chosen in order to maximize both the completeness (avoid missing real identifications) and reliability (keep spurious identifications as low as possible) of the associations.

2.2.1 *Results*

In this section we present the final multiwavelength catalogue created by cross-correlating the IRAC catalogue with the optical and the MIPS catalogues. For the sources with no 5σ i^+-band counterpart we have performed a match with the K_s-band catalogue.

(i) *IRAC + Optical*. We considered sources in the optical catalogue with flux in the i^+ band $>5\sigma$, and eliminated the masked areas and the stars from both catalogues. We performed a match through the likelihood ratio method considering a maximum radius of 3 arcsec (in order to maximize the overdensity around the IRAC position) and a dispersion of $\sigma = 1$arcsec for the distribution of the positional errors. The distribution of the *background*, the *total* and the *real* counts is shown in Fig. 1.

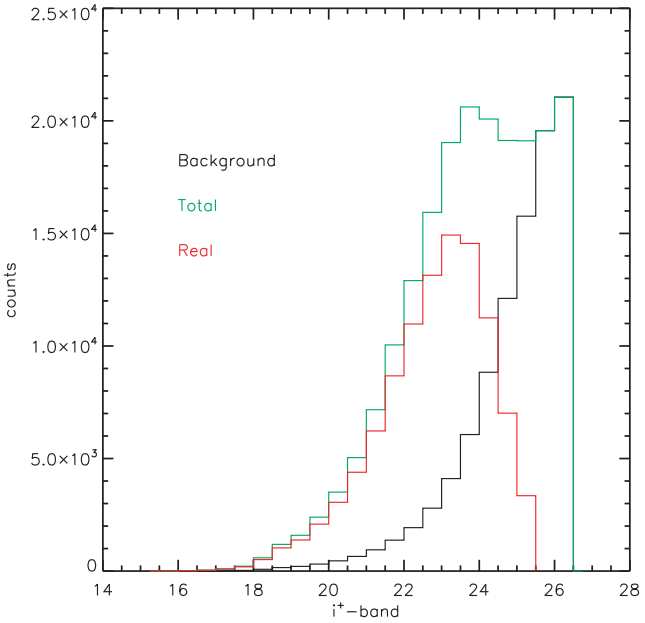

Figure 1. Magnitude distribution of the background (black line), total (green line) and real counts (red line) in the i^+ band.

The majority (96 per cent) of the associations have a separation $\leq$1 arcsec, with the median separation being $\sim$0.34 arcsec. For a non-negligible fraction of the associations with a separation $>$1 arcsec, the photometric redshift we obtained (see Section 3) was not in agreement with the spectroscopic one, meaning a probable spurious IRAC-optical association. Therefore, we have considered as reliable only matches within a separation of 1 arcsec, which is a standard separation used in literature when cross-correlating optical and IRAC catalogues. To reduce contamination from active galactic nuclei (AGN) we have also eliminated the IRAC sources with an optical counterpart associated to an X-ray detection with *XMM–Newton* (1.5 per cent of the IRAC sample). Finally, we obtained a reliable optical counterpart for 74 742 IRAC sources (95 per cent). We will refer to these sources as the 'optical subsample' hereafter.

(ii) *IRAC+24 μm*. We found 11 352 IRAC sources (14 per cent) with a reliable MIPS counterpart detected at 5σ. The likelihood ratio method, as described above, has been used.

(iii) *IRAC+K_s*. For the sources without an optical counterpart we have performed a match with the K_s-selected catalogue. In this case we used the nearest neighbour technique with a maximum separation of 1 arcsec. The similar wavelengths of the K_s and IRAC1 bands allows to perform this match with a low probability of misidentification. 90 per cent (3554 sources over 3907) of the IRAC sources with no optical counterpart, have a K_s counterpart ('K_s subsample' hereafter). As already mentioned, the K_s-band catalogue from McCracken et al. (2010) contains also information in additional bands (B_J, i^+, z^+ and J). The median magnitude in the i^+ band of these sources is $i^+ \sim 26$, i.e. these sources are optically very faint, consistent with them being not in the 'optical subsample'.

Finally, we have 353 sources for which we did not find neither an i^+-band counterpart, nor a K_s counterpart and for which we have only the IRAC bands information ('IRAC subsample' hereafter) and, eventually, the 24 μm (50 sources). The results of the cross-correlation and the final numbers of our catalogue are summarized in Table 1.

Table 1. Number of sources detected in the optical, K_s and MIPS catalogues.

	N (per cent of the whole sample)	MIPS detection
IRAC sample (all)	78 649	11 352
Optical subsample	74 742 (95 per cent)	10 779
K_s subsample	3554 (4.5 per cent)	523
IRAC subsample	353 (0.5 per cent)	50

3 PHOTOMETRIC REDSHIFT

The only efficient way to estimate the redshifts of the galaxies for the whole sample, given the large number of sources considered, is to determine their photometric redshifts through a detailed SED-fitting procedure.

Photometric redshifts were derived using the LE PHARE code (Arnouts et al. 2001; Ilbert et al. 2006), which computes photometric redshifts based on a simple χ^2 template-fitting procedure. We used the COSMOS SED library provided by Ilbert et al. (2009), which contains a set of templates composed of ellipticals and spirals from the Polletta et al. (2007) library and also includes blue galaxies from the Bruzual & Charlot (2003) population synthesis models. We added six simple stellar population (SSP) models of different ages (0.05, 0.5, 1.0, 1.5, 2.0 and 3.0 Gyr) from Maraston (2005) to account for passively evolving galaxies at high redshifts. The final library is composed of seven ellipticals, twelve spirals, twelve starbursts and six SSP templates. Some representative templates of the library are shown in Fig. 2. This set of templates maximizes the accuracy of the derived photometric redshifts (z_p) when compared with the available spectroscopic redshifts (z_s) (see Section 3.1).

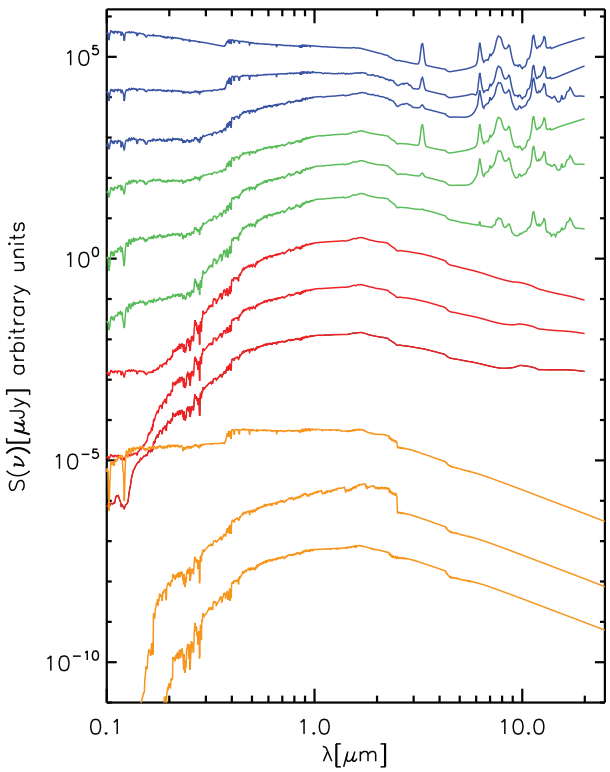

Figure 2. Representative templates of the SED library. Orange: simple stellar population models of 0.05, 1.0 and 3.0 Gyr (Maraston 2005). Red: elliptical (Polletta et al. 2007). Green: spirals (Polletta et al. 2007). Blue: blue galaxies (Bruzual & Charlot 2003).

Table 2. 5σ limit adopted for each band.

Band	Optical subsample	K_s subsample
u^*	25.3	–
b_J	25.7	27.0
g^+	25.5	–
V_J	25.5	–
r^+	25.6	–
i^+	25.1	26.2
z^+	24.5	25.0
J	22.0	22.0
K	22.0	–
IRAC1	–	–
IRAC2	23.3	–
IRAC3	21.2	–
IRAC4	21.0	–
MIPS	18.5	–

We allowed three different extinction laws (Calzetti et al. 2000, Calzetti modified and Prevot et al. 1984) to be applied to each template. The Calzetti modified extinction law includes an ultraviolet (UV) bump at 2175 Å (Ilbert et al. 2009), which is fundamental to have good z_p at $z > 1.5$. We used nine different values of $E(B-V)$: 0, 0.05, 0.1, 0.15, 0.2, 0.25, 0.3, 0.4 and 0.5.

We set an upper limit (5σ) to each band when there is no detection, as shown in Table 2. This 5σ limit has been chosen following a conservative approach, i.e. as the brightest magnitude value of the sources in the catalogue detected with S/N = 5. We fitted our data from the U to the 24-μm band. The χ^2 minimization procedure is highly affected by the adopted photometric errors (see Ilbert et al. 2009 for a detailed discussion of the issue). We have increased the flux error by 6, 5 and 8 per cent for the optical, IRAC and MIPS bands, respectively.

3.1 Photometric redshift accuracy

We were able to test the quality of our derived photometric redshifts for the IRAC sources with i^+-band detection by comparison with a large sample of spectroscopic redshifts. In particular, we made use of 8176 sources with derived spectroscopic redshift at a very high confidence level (99.8 per cent, flags 3.1, 3.5, 4.1, 4.5) from the zCOSMOS faint and bright surveys (Lilly et al. 2007, 2009). We estimated the redshift accuracy as $\sigma_{\Delta z/(1+z_s)}$ (where $\Delta z = z_p - z_s$ is the difference between the photometric and the spectroscopic redshifts) using the normalized median absolute deviation defined as $1.48\langle|z_p - z_s|/(1+z_s)\rangle$. We also defined the percentage of catastrophic errors, η, as the objects with $|z_p - z_s|/(1+z_s) > 0.15$. We obtained an accuracy of $\sigma_{\Delta z/(1+z_s)} = 0.060$ and a percentage of catastrophic failures of $\eta = 3.3$ per cent as can be seen in Fig. 3. As a comparison, Ilbert et al. (2009) using the bright ($i^+ < 22.5$ mag) sample with 30 bands and narrow filters obtained $\sigma = 0.007$ and <1 per cent of catastrophic errors for their derived photometric redshifts, while the average value of σ obtained by Pérez-González et al. (2008) using an IRAC selected catalogue with data from the UV to the MIR is 0.055. Given the fact that we use 14 broad bands, we find our result comparable to those in literature.

We also tested the reliability of our z_p for the faintest sources, with $\mathrm{mag}_{3.6\,\mu m} > 21.0$ and $i^+ > 22.5$, as shown in Figs 4 and 5. The value of σ for the faint i^+-band sources ($\sigma = 0.057$) is comparable to the value of σ for the whole sample, while the number of catastrophic

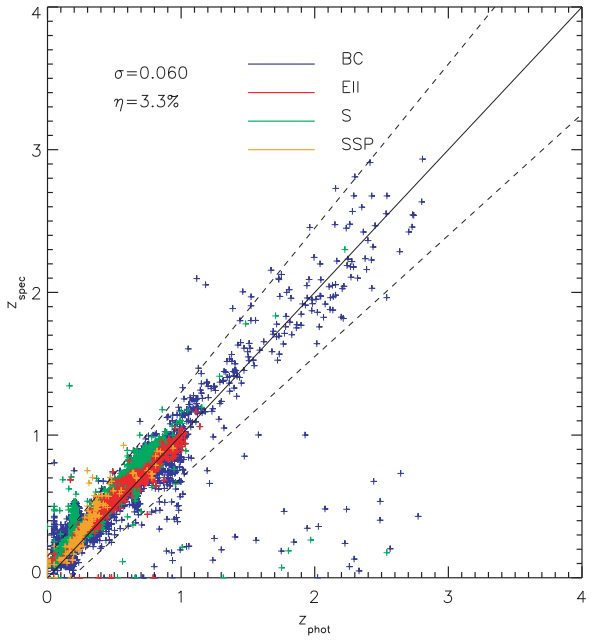

Figure 3. Comparison between z_p and z_s for the 8176 sources with optical and IRAC detection of the zCOSMOS sample. The value of σ and η are shown in the plot. The different colours represent sources fitted by different SED templates as explained in Fig. 2. Dashed lines represent $|z_p - z_s|/(1 + z_s) = 0.15$, i.e. sources out of that region are considered as catastrophic errors.

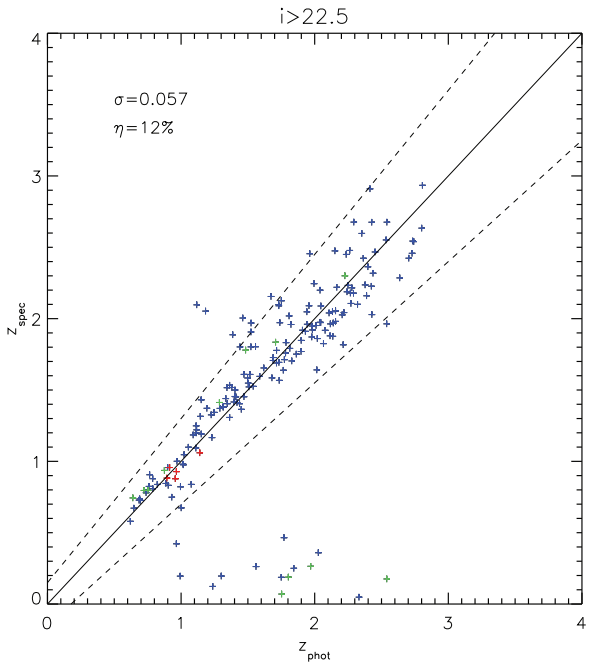

Figure 4. Comparison between z_p and z_s for 183 sources with i^+ band > 22.5. Colours and dashed lines as in Fig. 2.

errors increases ($\eta = 12$ per cent). For the faint IRAC1 sample both σ and η are smaller than for the whole sample ($\sigma = 0.037$, $\eta = 1.9$ per cent). This may surprise the reader, but it must be noticed that the values for the whole spectroscopic sample are highly affected by a significant dispersion on low-redshift sources ($z_s \sim 0.3$–0.5,

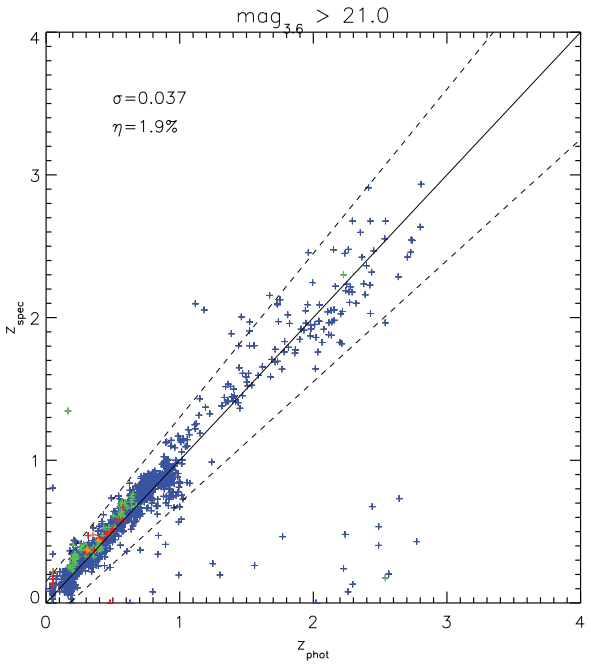

Figure 5. Comparison between z_p and z_s for 2381 sources with $\mathrm{mag}_{3.6\,\mu m} > 21.0$. Colours and dashed lines as in Fig. 2.

see Fig. 3), which are present in a smaller fraction in the faint IRAC sample.

3.2 Photometric redshift accuracy for the IRAC sources with no *I*-band counterparts

For the sources with no i^+-band counterpart it is not possible to directly compare the photometric redshifts with spectroscopic redshifts, since no z_s are available for these sources. To test the quality of the derived photometric redshifts we have made use of the 1σ dispersion of the z_p distribution, given as an output of the LE PHARE code. The mean error on the z_p for the whole sample is $\sigma_z = 0.17$, which corresponds to $\sigma_{\Delta z/(1+z_s)} \sim 0.057$ at $z \sim 2$, meaning that the 1σ dispersion of the z_p distribution is consistent with the $\sigma_{\Delta z/(1+z_s)}$ derived from the z_p and z_s comparison. The redshift uncertainties derived from LE PHARE have been used in the Monte Carlo simulations (see Section 7).

In Figs 6, 7 and 8 we show some examples of SED fitting for sources fitted by different templates [elliptical (Ell), SSP, spirals (S) and blue galaxies or starbursts (SB)] for sources from the optical, K_s and IRAC subsamples.

3.3 Redshift distribution

Fig. 9 shows the redshift distribution for each subsample, highlighting the contribution from different classes of best-fitting templates. Templates have been divided in three classes: elliptical/old SSP (older than 1 Gyr), blue/young SSP (younger than 1 Gyr) and spirals. It can be observed that these redshift distributions are not smooth, but show some peaks at given redshifts, e.g. at $z \sim 1.0$, 2.0 for the K_s subsample or a very prominent peak at $z \sim 4.0$ for the IRAC subsample. Note that the peak at $z \sim 4$ in the IRAC subsample is not used in this paper since we limit our analysis to $z < 3.0$ and also the small number of sources involved in this peak (<0.2 per cent of the sample). This kind of features in the redshift distribution

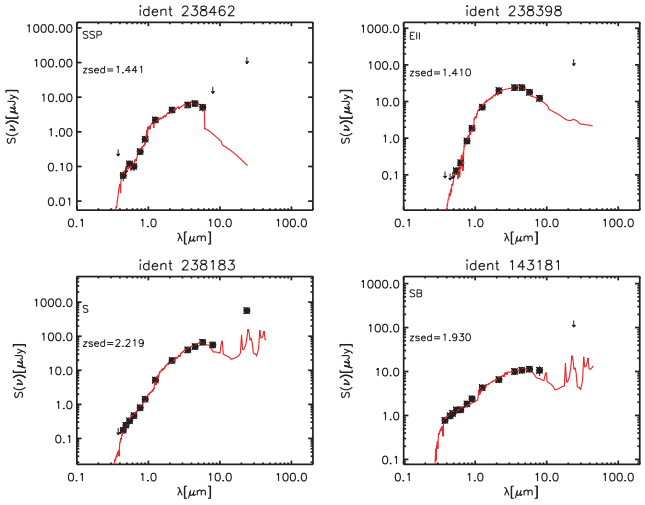

Figure 6. Example of SED fitting for four sources from the optical subsample. The observed SED of each source (black filled circles) is shown with the corresponding best-fitting solution (red solid line), as well as the derived z_p and best template model. Arrows represent upper limits (5σ) when no detection is found in that band.

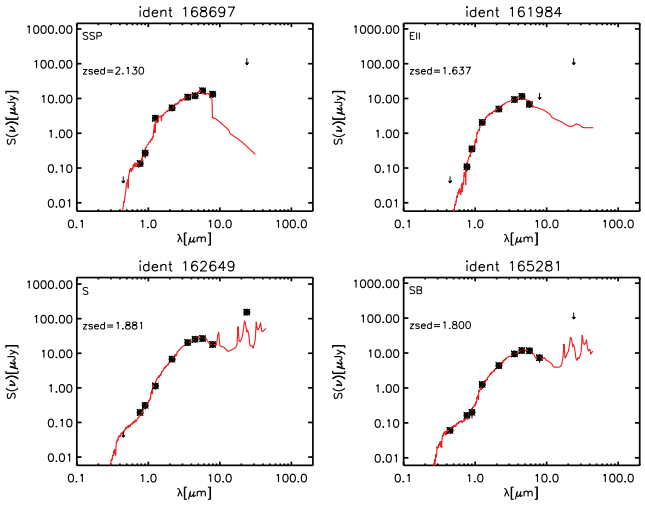

Figure 7. Example of SED fitting for four sources from the K_s subsample, i.e. sources not present in the i^+-band catalogue (Ilbert et al. 2010) but with a K_s counterpart (McCracken et al. 2010).

are presumably not real, but due to the determination of the redshifts through a SED fitting procedure. Spiky redshift distributions have also been reported in literature, e.g. by Pérez-González et al. (2008) and Franx et al. (2008) among others. The number of sources in each subsample with a reliable z_p is shown in Table 3, as well as the number of sources for each subsample fitted with each class of template. The number of high-redshift ($z \gtrsim 1.4$ and 2.5) sources for each subsample is also shown.

It is clear how differently the three subsamples behave, with 88 and 91 per cent of the K_s and the IRAC subsamples respectively found at high redshift ($z \geq 1.4$), in comparison to 21 per cent of the optical subsample. For very high redshift sources ($z \gtrsim 2.5$) the differences are even more significant, since only 2.3 per cent of the optical subsample is found at those redshifts, while this percentage is 27 and 47 per cent for the K_s and IRAC subsamples, respectively. Also the relative fractions of best-fitting templates are very different.

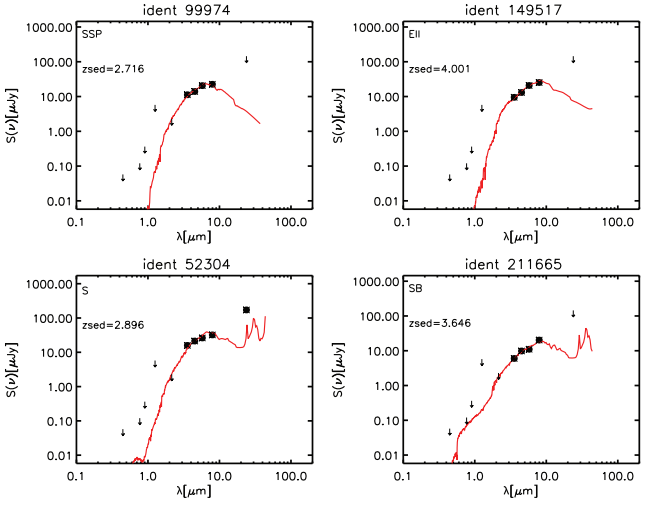

Figure 8. Example of SED fitting for four sources from the IRAC subsample, i.e. sources only detected in the IRAC bands.

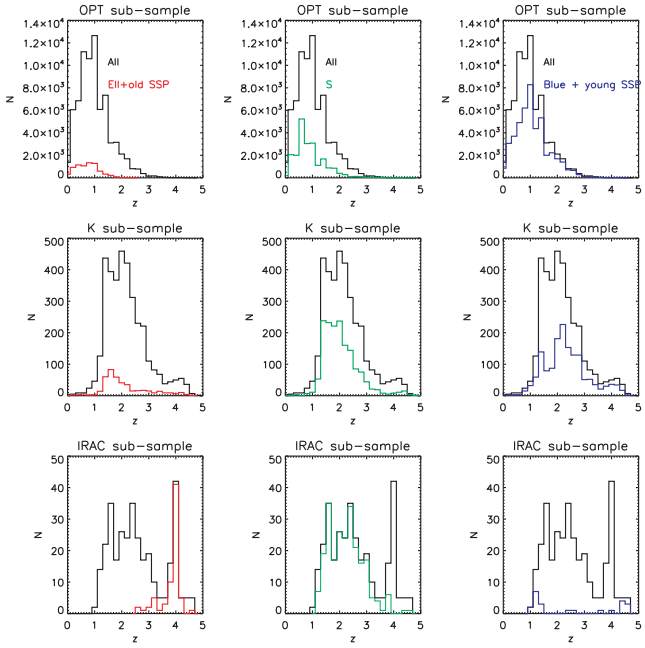

Figure 9. Redshift distribution for the different subsamples. In the three upper panels we show the redshift distribution of the optical subsample (black line), as well as the redshift distribution of the sources fitted by an elliptical/old SSP template (red line), a spiral template (green line) or a blue/young SSP template (blue line). The same is plotted for the K_s and the IRAC subsamples in the middle and bottom panels, respectively.

On the one hand, 10 per cent of the optical subsample is fitted by an elliptical/old SSP model, while for the IRAC subsample the fraction is double (22 per cent). On the other hand, only 7 per cent of the IRAC subsample is fitted by a blue/young SSP model, while these templates represent 62 per cent of the solutions for the optical subsample. These percentages are indicative of the importance of an IRAC selected sample to study the properties of high-redshift galaxies whose SED is reproduced by quiescent populations.

Table 3. Percentages of best-fitting templates and high redshift sources ($z \geq 1.4$ and 2.5) for the different subsamples.

	Optical subsample	K_s subsample	IRAC subsample
All	74 742	3554	328
Ell/old SSP	10 per cent	12 per cent	22 per cent
S	28 per cent	45 per cent	71 per cent
Blue/young SSP	62 per cent	43 per cent	7 per cent
$z \geq 1.4$	21 per cent	88 per cent	91 per cent
$z \geq 2.5$	2.3 per cent	27 per cent	47 per cent

4 GALAXY STELLAR MASSES

To study the evolution of the GSMF of sources at high redshift we have selected the sources with $z \geq 1.4$. When available, we have made use of z_s (654 out of 19 042 sources, ∼3.4 per cent of the sample).

The galaxy stellar masses have been derived by means of the LE PHARE code by fitting our data (up to 5.8 μm) with a set of SED templates from Maraston (2005) with SFH exponentially declining with time as SFR $\propto e^{-t/\tau}$. We used nine different values of τ (0.1, 0.3, 1.0, 2.0, 3.0, 5.0, 10.0, 15.0 and 30.0 Gyr) with 221 steps in age. The metallicity is solar and the IMF Chabrier. Dust extinction was applied using the Calzetti et al. (2000) extinction law, with a maximum $E(B-V)$ value of 0.5. We imposed to the derived age of the galaxies to be less than the age of the Universe at that redshift and greater than 10^8 yr (the latter requirement avoids having galaxies with extremely high specific star formation rates, SSFR = SFR/M (SSFR hereafter)). The Maraston (2005) models include a better treatment of the thermally pulsing asymptotic giant branch (TP-AGB) phase, which has a high impact on modelling the templates at ages in the range $0.3 \lesssim t \lesssim 2$ Gyr, where the fuel consumption in this phase is maximum, specially for the NIR part. Although some authors (Kriek et al. 2010) have recently claimed that the Maraston (2005) models do not properly reproduce the observed data in a sample of post-starburst galaxies, i.e. at the time when TP-AGB stars are thought to be most dominant, we have instead found good fits for our SEDs. Pozzetti et al. (2010) measured an average systematic shift of 0.14 dex between the stellar masses computed with the Bruzual & Charlot (2003) models and the Maraston (2005). We will take into account this difference when comparing our results with those obtained with the Bruzual & Charlot (2003) models.

Uncertainties in the stellar mass derivation are due to a number of different assumptions in the SED fitting procedure, like, for example, the use of different IMF, extinction laws, metallicities, SFH or SED template libraries. Tests on simulated catalogues considering the effect on stellar mass estimates of different choices of reddening laws SFHs, metallicities and SED libraries show a typical dispersion of the order of $\sigma(\log M) \sim 0.20$ (see Bolzonella et al. 2010), showing that the stellar mass is a rather stable parameter in the SED fitting.

The mean error on the stellar mass, as estimated from the 1σ dispersion of the mass distribution (given as an output of the LE PHARE code), is 0.16 dex, consistent with the uncertainties mentioned above.

5 GALAXY CLASSIFICATION

We are interested in studying the characteristic evolution of the quiescent and star-forming galaxies. To discriminate between these two types, we have made use of a classification based on the SSFR derived through the SED-fitting process. We considered three different populations.

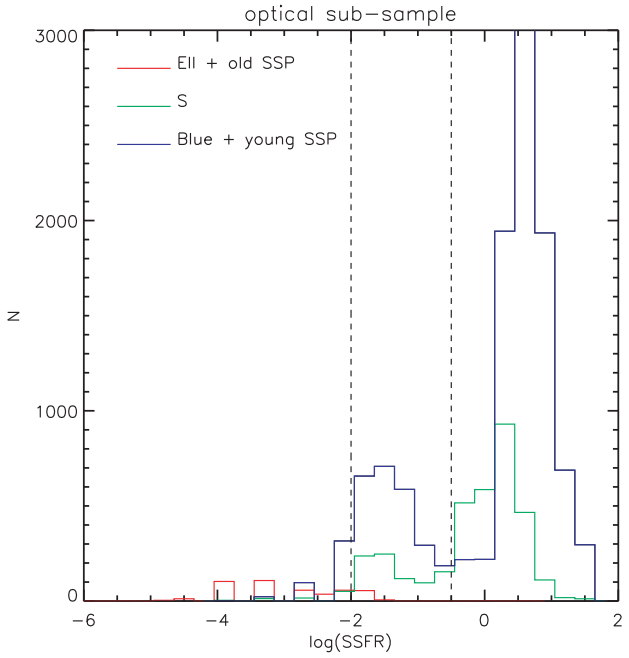

Figure 10. SSFR distribution for the optical subsample of sources with $z \geq 1.4$. The colours represent the different classes derived from the SED fitting templates. Dashed vertical lines represent the limits considered in SSFR to divide sources as actively star forming, intermediate or quiescent.

(i) Actively star-forming galaxies: those for which log(SSFR [Gyr^{-1}]) > -0.5.

(ii) Intermediate galaxies: those for which $-2 <$ log(SSFR [Gyr^{-1}]) < -0.5.

(iii) Quiescent galaxies: those for which log(SSFR [Gyr^{-1}]) < -2.

We found 84 sources (∼0.5 per cent of the high-redshift sample, i.e. sources with $1.4 \leq z \leq 3.0$) with log(SSFR[Gyr^{-1}]) < -2 and detected in the 24-μm band. As the emission at 24 μm usually arises from dust heated by star formation activity, we include these sources in the intermediate population.

The limits on the SSFR values have been defined from the distribution of the SSFR values (Fig. 10 for the optical subsample) and we have verified that they are consistent with the best-fitting template classification. Most of the sources with very low SSFR are fitted by an elliptical or old SSP template, while those with the highest activity are generally fitted by a young SSP or a blue template, as should be expected on the basis of their colours. Considering the whole sample, we have carefully studied the cases where star-forming sources are fitted by an elliptical or old SSP template, as well as quiescent sources fitted by a blue or a young SSP template. We found only 26 sources ($\lesssim 0.1$ per cent of the high-redshift sample) fitted by an elliptical or old SSP template with high activity. On the other hand, more than 94 per cent of the 639 sources (3.5 per cent of the high-redshift sample) fitted by a blue template with low SSFR are not detected in the U band, which is a critical band to determine the star formation activity of a galaxy.

In Table 4 we report the number of galaxies classified as star forming, intermediate and quiescent, as well as the MIPS detected sources, in each redshift bin for sources with $1.4 \leq z \leq 3.0$.

Table 4. Number of galaxies with $1.4 \leq z \leq 3.0$ in each redshift bin as classified by the SSFR.

z	All	Quiescent	Intermediate	Star forming	MIPS
1.4–1.6	5142	515	1325	3302	261
1.6–2.0	6303	512	1445	4346	1286
2.0–2.5	4693	287	914	3492	1178
2.5–3.0	1794	77	415	1302	272

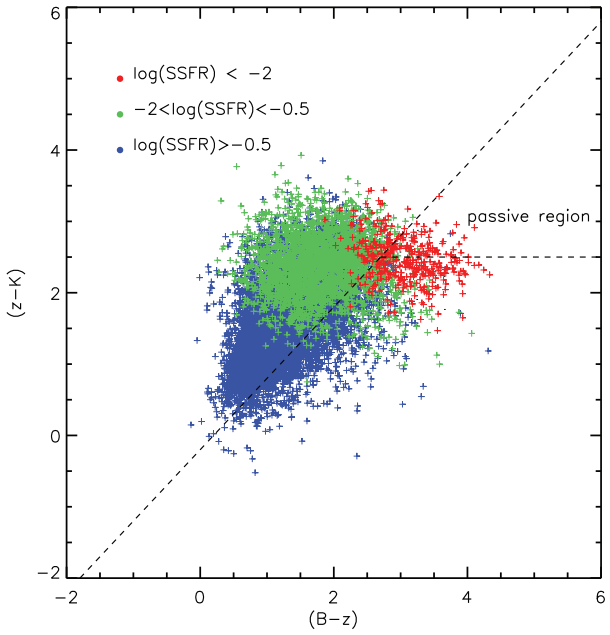

Figure 11. *BzK* diagram (Daddi et al. 2004) for optically detected sources with $1.4 \leq z \leq 2.5$. The colours represent the different classes derived from the SSFR criteria (red: quiescent, green: intermediate, blue: star forming). The dashed lines show the different regions of the *BzK* diagram.

Other tests, such as the *BzK* classification (Daddi et al. 2004), which separates star-forming and quiescent galaxies with respect to their $(B - z)$, $(z - K)$ colours for sources with $1.4 \leq z \leq 2.5$, shows that galaxies for which low activity is derived roughly occupy the passive region in the *BzK* diagram $[(z - K) - (B - z) < -0.2$ and $(z - K) > 2.5]$, while for the star-forming galaxies, their colours are consistent with the *BzK* star-forming selection (Fig. 11). Only three sources defined as active star forming fall in the passive region of the *BzK* diagram.

The lack of detection in some bands worsens the derived SSFR, thus complicating a precise classification. We have derived mean SSFR errors making use of the 1σ dispersion of the SSFR distribution, obtaining a mean SSFR error of 0.38 dex for the whole sample.

6 PROPERTIES OF HIGH-Z QUIESCENT GALAXIES

The evolution over the cosmic time of quiescent galaxies represents a key tool to understand the galaxy mass assembly. In this section we summarize the properties of the high-redshift quiescent galaxies (also known as ETGs in literature) by analysing the physical parameters obtained through the SED-fitting procedure.

We find 1455 quiescent galaxies at $z \geq 1.4$. They are old and massive galaxies ($\langle M \rangle \sim 10^{10.65}\,\mathrm{M}_{\odot}$): more than 56 per cent of them have $M \geq 10^{10.6}\,\mathrm{M}_{\odot}$ and ∼12 per cent have $M \geq 10^{11.0}\,\mathrm{M}_{\odot}$. They have weakly star-forming stellar populations, with ages ranging from 1–4.25 Gyr. Some of them are so old to reach the limit allowed by the age of the Universe at their redshift, meaning very high formation redshifts. They have e-folding time-scales $\tau \sim$ 0.1–0.3 Gyr, i.e. they should have formed in a very intense and brief starburst. They are characterized by very low dust extinction $(E(B - V) \sim 0 - 0.15)$, implying that their red optical colours are due to evolved stellar populations and not to dust extinction. These characteristics are in agreement with previous results (e.g. Kriek et al. 2008; Cimatti 2009).

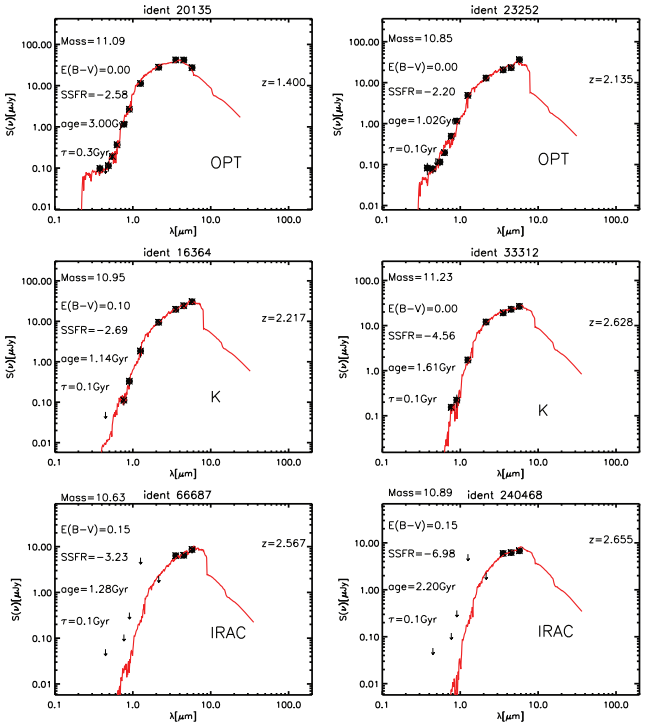

Figure 12. SED fitting of some high-redshift quiescent galaxies. Also shown the main physical parameters derived through the SED-fitting process (mass, extinction, SSFR, age, τ, z). The OPT, K_s and IRAC labels indicate the subsample at which each source belongs.

In Fig. 12 we show the SED fitting and main physical parameters of six different high-redshift quiescent galaxies. We show examples from the optical, K_s and IRAC subsamples. We underline the importance of the upper limits in the optical and K_s bands for the IRAC subsample to constrain the SED model.

7 THE GALAXY STELLAR MASS FUNCTIONS

We study the evolution of the quiescent galaxies by deriving their mass function in four redshift bins. The mass function of the whole sample and of the star forming and intermediate galaxies are also estimated to compare the evolution of the different populations. The classical non-parametric $1/V_{\mathrm{max}}$ formalism (Schmidt 1968) has been used and data have been fitted to a Schechter function (Schechter 1976). The GSMF is computed only in the non-masked regions with a total covered area of 1.73 deg^2.

Estimating the stellar mass limit for a magnitude limited sample is not straightforward due to the high range of possible M/L ratios for different galaxy populations and colours. To account for this effect we define, at each redshift, a minimum mass, M_{min}, above

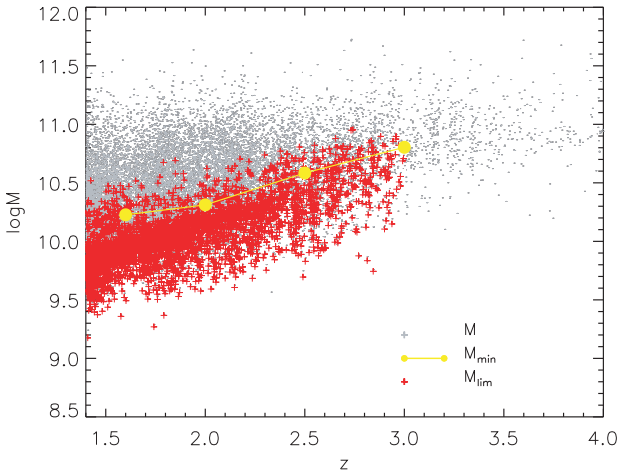

Figure 13. Stellar mass as a function of redshift (small grey dots). Red crosses are the $M_{\rm lim}$ of the 20 per cent faintest galaxies at each redshift, while $M_{\rm min}(z)$ are plotted as yellow circles.

which the derived GSMF is essentially complete because all types of galaxies are potentially observable above this mass.

Following Pozzetti et al. (2010), we calculated for each galaxy its limiting stellar mass, i.e. the mass it would have at its redshift if its observed magnitude were equal to the limiting magnitude of the sample ($\rm mag_{3.6lim} = 22.0$); $\log(M_{\rm lim}) = \log(M) + 0.4(\rm mag_{3.6} - mag_{3.6lim})$. In order to derive a representative limit for our sample we used the $M_{\rm lim}$ of the 20 per cent faintest galaxies at each redshift. We then defined the $M_{\rm min}(z)$ as the upper envelope of the $M_{\rm lim}$ distribution below which lie 95 per cent of the $M_{\rm lim}$ values at each redshift. This $M_{\rm min}$ corresponds to a 95 per cent completeness limit at each redshift. The distribution of mass with redshift, as well as the $M_{\rm lim}$ and the $M_{\rm min}(z)$ calculated as explained above are shown in Fig. 13.

Fig. 14 presents the total and the quiescent GSMF (QSMF hereafter) of our IRAC selected sample in four different redshift bins: 1.4–1.6, 1.6–2.0, 2.0–2.5 and 2.5–3.0. At $z > 3.0$ the uncertainties become dominant so we decided to limit our analysis to $z \leq 3.0$. The circles represent the GSMF for all the sources, while the lines show the best Schechter function fitting our data. The Poissonian errors have been computed assuming Poissonian statistics (Zucca et al. 1997):

$$\sigma = \left[\sum_i \left(\frac{1}{V^2_{\rm max}(M_i)}\right)\right]^{1/2}. \quad (3)$$

However, the Poisson errors in our GSMF are an underestimate of the real uncertainties, since they do not take into account how the $z_{\rm p}$ uncertainties propagate on the GSMF. This uncertainty is especially important for the optically undetected sources, therefore we have to be very careful in the z-bins where these sources dominate (higher redshift). To assess for this uncertainty we have performed Monte Carlo simulations. We have created 20 mock catalogues by randomly picking a redshift within the redshift probability distribution function (PDFz) of each object (given by LE PHARE code), we have recalculated the mass and other important physical parameters and we have computed the GSMF for each of the 20 mock catalogues. We have then calculated the 1σ dispersion of the GSMF values at each mass and redshift bin. The cosmic variance is another important source of uncertainty. Following the formalism of Somerville et al. (2004) we have derived $\sigma_{\rm cv} \sim 0.18, 0.14, 0.14$ and 0.16, respectively, in the four redshift bins. Finally, we added in quadrature these errors to the Poissonian errors (yellow area in Fig. 14). The red area represents the upper and lower limits of the QSMF calculated in the same way as for the total GSMF.

7.1 Comparison of the total GSMF with literature

In Fig. 14 we show for comparison the GSMF derivations from the literature (blue triangles from Pérez-González et al. 2008, green asterisks from Fontana et al. 2006, red diamonds from Marchesini et al. 2009, orange squares from Ilbert et al. 2010). All GSMF's were converted to Chabrier IMF and shifted by -0.14 dex in mass (to account for the difference in the derived mass when using Maraston 2005 or Bruzual & Charlot 2003 models, see Pozzetti et al. 2010). We are in reasonably good agreement with many of the other results. However, a significant difference is observed in all redshift bins at high masses with respect to the results of Pérez-González et al. (2008), as they found a number density significantly higher than ours. With respect to Marchesini et al. (2009), we find less massive galaxies at $z < 2$ and more intermediate mass ($\log M \sim 10.5$) galaxies at $2 < z < 2.5$. The agreement with Ilbert et al. (2010), whose sample is also IRAC selected in the COSMOS field, is very good, with small differences probably arising from different redshift binning, as it may happen also with Fontana et al. (2006). However, we have a slight overdensity of intermediate mass galaxies ($M \sim 10^{10.7}\,\rm M_\odot$) at $2.0 < z < 2.5$ when compared with all other results from literature, which may be too big to be explained only by differences in redshift binning.

In comparison with other authors, we are using data from the COSMOS survey, which is the largest studied area ($\sim$1.7 deg^2) with full multiwavelength coverage.

7.2 The evolution of the quiescent galaxies

In Fig. 15 the QSMF obtained in the four studied redshift bins is reported. The shaded areas represent the upper and lower limits, derived as explained in Section 7, while the thick lines are the Schechter fitting to our data.

We observe a significant evolution of the QSMF from $2.5 < z < 3.0$ to $1.4 < z < 1.6$, increasing $\sim$1 dex for galaxies with $\log M \sim 11.0$ in the redshift interval studied. The evolution is $\sim$0.3 dex in each redshift bin, meaning that the number of quiescent galaxies continuously increases with cosmic time.

In Fig. 16 we compare the GSMF derived for quiescent galaxies, with those of the other populations. The red, green and blue areas represent the quiescent, intermediate and actively star-forming populations, respectively. We also show for comparison the results obtained by Ilbert et al. (2010), with purple, dark green and light blue circles representing their quiescent, intermediate and high-activity galaxies, respectively. The agreement is good for the quiescent population in both redshift bins in common (1.4–1.6, 1.6–2.0), while the differences for the intermediate and star-forming population can be explained by the different classification methods used. While for the quiescent population we used a similar cut in SSFR, for the cut between the intermediate and high-activity populations they used $\log(\rm SSFR[Gyr^{-1}]) \sim -0.3$, while we are using a value of -0.5.

The evolution of the star-forming galaxies is quite complex (see Fig. 16). They remain almost constant from $2.5 < z < 3.0$ to $2.0 < z < 2.5$, being the dominant population at all masses in those redshift bins. However, their number density decreases when moving to the lowest redshift bins and this decrease depends on the galaxy mass:

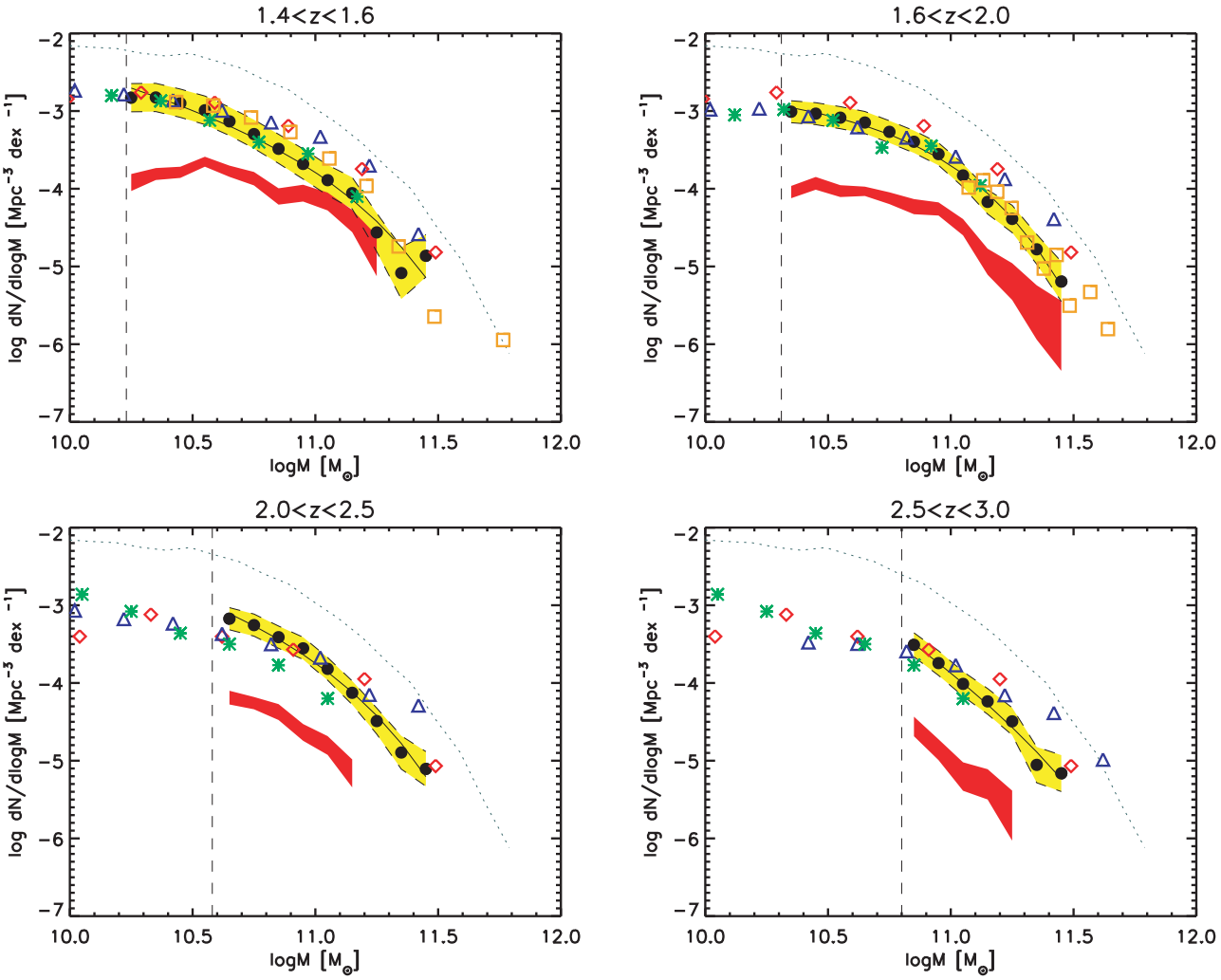

Figure 14. Stellar mass function in four redshift intervals for the quiescent (red area) and the total (yellow area) sample. Our estimates at each redshift for the whole sample are plotted as filled black circles. Data are fitted with a Schechter function (solid lines). The coloured areas represent upper and lower limit of the total and quiescent mass functions as derived from the combination of the Monte Carlo simulations, cosmic variance and Poissonian errors. Black dotted line: local MF (Cole et al. 2001). Dashed vertical lines represent the completeness in mass for each redshift bin. GSMFs from other authors are also plotted: blue triangles from Pérez-González et al. (2008), green astrerisks from Fontana et al. (2006), red diamonds from Marchesini et al. (2009), orange squares form Ilbert et al. (2010).

while for high masses we observe a significant decline (∼0.8 dex for $\log M \sim 11.0$), for low masses ($\log M \sim 10.5$) the GSMF is almost constant. A decrease of the star-forming population from $1.6 < z < 2.0$ to $1.4 < z < 1.6$ is in agreement with the results of Ilbert et al. (2010) and, as reported in studies at lower redshift (see for example Pozzetti et al. 2010; Ilbert et al. 2010), the number of star-forming galaxies continues to decrease to almost local redshift ($z \sim 0.1$). The intermediate population constantly increases its number at all masses, first at high masses (∼0.2 dex from $2.5 < z < 3.0$ to $1.6 < z < 2.0$ for $\log M \sim 11.0$), then at low masses (∼0.2 dex from $1.6 < z < 2.0$ to $1.4 < z < 1.6$ for $\log M \sim 10.5$). This means that they become more abundant than the star-forming population at $\log M \gtrsim 10.6$ at $1.4 < z < 1.6$. Finally, as mentioned before, for the quiescent population we find an increase of ∼1 dex in the number density from $2.5 < z < 3.0$ to $1.4 < z < 1.6$ for $\log M \sim 11.0$. At the lowest redshift bin ($1.4 < z < 1.6$) the quiescent population becomes more important than the active one for masses $\log M \gtrsim 10.75$.

Considering all the populations, we find that $z \sim 1.5$ is a clear epoch of transition of the GSMF: while the GSMF at $z \gtrsim 1.5$ is dominated by the actively star-forming galaxies at all stellar masses, at $z \lesssim 1.5$ the contribution to the total GSMF of the quiescent galaxies is significant and both the intermediate and the quiescent population become more important than the star-forming one for $M \geq 10^{10.75}\,\mathrm{M}_\odot$.

In Table 5 we report the best-fitting Schechter parameters for the quiescent sample. In the last redshift bin ($2.5 < z < 3.0$) the Schechter fit failed to converge when leaving all the parameters free. We fixed the faint end slope α to its value at $2.0 < z < 2.5$ to be able to obtain the other Schechter parameters. While, given the large uncertainties, we cannot derive firm conclusions on the faint end slope α nor on M^*, we detect, as already mentioned, a significant increase of ϕ from $2.5 < z < 3.0$ to $1.4 < z < 1.6$.

We caution the reader that the uncertainties of this derived GSMF at such high redshift may change our results significantly due to the difficulties in estimating the z_p as well as the activity classification.

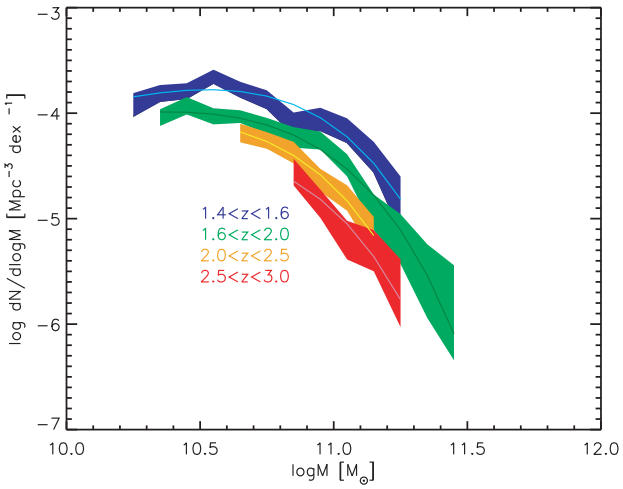

Figure 15. Evolution of the QSMF with redshift for different redshift bins. Blue: 1.4–1.6; green: 1.6–2.0 ; orange: 2.0–2.5; red: 2.5–3.0. Shaded regions represent the upper and lower limits of the GSMF for each redshift bin (see Section 7), while the thick lines are the Schechter fitting to the data.

8 DISCUSSION

To better understand the behaviour of the different populations we have plotted the fraction of quiescent/star-forming galaxies over the total versus mass for different redshift bins (Fig. 17). The fraction of the actively star-forming galaxies decreases from ∼60 to ∼20 per cent from $2.5 < z < 3.0$ to $1.4 < z < 1.6$ for $M \gtrsim 10^{11.0}\,\mathrm{M}_\odot$, while that of quiescent galaxies increases from ∼10 per cent to ∼50 per cent in the same redshift and mass intervals. The evolution is also mass-dependent, with the most massive galaxies becoming quiescent first, while at $M \lesssim 10^{10.5}\,\mathrm{M}_\odot$ the star-forming population still dominates the sample at all redshifts.

This trend suggests that actively star-forming galaxies, which dominate the sample at high redshifts (mainly at $z \gtrsim 2.0$), may quench their star formation and become less abundant at later time. This quenching of the star formation seems to be mass dependent, with the most massive galaxies quenching their star-formation first, while the less massive galaxies continue to form stars until later times. If the evolution of the star-forming galaxies should be that of becoming intermediate galaxies to finally end their lives as quiescent galaxies, the increase of this latter population at low redshifts could be explained, with the quiescent population being the dominant population at low redshift, as all galaxies may evolve to that type once their SF has stopped. Therefore, we could be unveiling the formation epoch of the very active galaxies and their following evolution from the blue cloud to the red sequence.

Fig. 18 shows the evolution of the fraction of quiescent galaxies with redshift for sources with $M \geq 10^{10.85}\,\mathrm{M}_\odot$ (red circles). The errors are a combination of the Monte Carlo simulations and Poissonian errors. For comparison, we also plotted the values obtained by Fontana et al. (2009, orange triangles) and from Damen et al. (2011, light blue diamonds), as well as the predictions of theoretical models (Menci et al. 2006, M06 hereafter; Kitzbichler & White 2007, K07; Nagamine et al. 2006, N06; Fontanot et al. 2007, F07). We observe a good agreement between the fraction of quiescent galaxies derived in this work and those from Fontana et al. (2009). The values of Damen et al. (2011) are also consistent with our results, although Damen et al. (2011) sources are selected with $M > 10^{11.0}\,\mathrm{M}_\odot$ and are defined as quiescent when SSFR $< 1/(3t_H)$. The fraction of massive quiescent galaxies increases from ∼8 to ∼35 per cent from $2.5 < z < 3.0$ to $1.4 < z < 1.6$, with the main evolution occurring between $1.6 < z < 2.0$ and $1.4 < z < 1.6$ (where the fraction increases from ∼18 to ∼35 per cent). This confirms the expected cosmological increase in number density of massive quiescent galaxies with cosmic time. All the theoretical models agree in predicting a gradual increase with time in the fraction of galaxies with low SFR, although large discrepancies between data and theoretical models are observed. It is beyond the scope of the present paper to give a detailed explanation of the differences between models, but we will discuss some generalities. Some models underpredict the fraction of quiescent galaxies at all redshifts, such as the purely semi-analytical models (M06, F07), and in particular predict virtually no such objects at $z > 2$, in contrast to what is observed. This lack of massive galaxies at high redshift for the model of F07 has already been noticed by Fontanot et al. (2007), who admitted that the downsizing trend of the galaxies is not fully reproduced yet in these models, and suggested that some kind of feedback mechanism could help to reproduce the data. A slightly higher fraction of quiescent massive galaxies is predicted by M06, as they include AGN feedback mechanism, due to the growth of supermassive black holes and the AGN triggered by interactions in the host galaxies. This AGN feedback enhances the fraction of galaxies populating the red branch of the colour distribution and is particularly effective at high z. However, it is not effective enough to reproduce the observed data at $z < 2.0$. The purely hydrodynamical model by Nagamine et al. (2006), represented with a shaded area for three different time-scales τ of the star formation rate (ranging from 2×10^7 to 2×10^8 yr), appears to overpredict the fraction of high-mass quiescent galaxies. The disagreement in the stellar mass density at $z > 1$ between these models and the observations has already been commented by Nagamine et al. (2006). The semi-analytical rendition of the Millennium N-body dark matter simulation by Kitzbichler & White (2007) is the only one which agrees with our observed data, being able to reproduce both the normalization and the shape of the increase in the fraction of quiescent massive galaxies with decreasing redshift. This model introduces radio mode feedback from the central galaxies of groups and clusters, which seems to be fundamental for the predictions to be consistent with the observations.

Finally, the non negligible fraction of quiescent galaxies at $z > 1.8$ implies that these galaxies assembled most of their stellar mass either during an active starburst phase or through important merging processes at higher redshifts. These star formation episodes must be quenched either by efficient feedback mechanism and/or by the stochastic nature of the hierarchical merging process.

In Figs 19 and 20 we have calculated the evolution of the stellar mass density with cosmic time for the quiescent sample (red symbols) and the intermediate plus the star-forming samples (dark blue). The values have been obtained in two different ways. The data plotted as squares represent the integral of the Schechter function fitting our data, including the extrapolations to the fainter masses. The diamonds are the sum of the data at all masses. As expected, the latter values are lower (since data are incomplete at low masses) but the two estimates are consistent within ∼0.18 dex. We do not show the value of the stellar mass density for the intermediate and star-forming galaxies in the redshift bins 2.0–2.5 and 2.5–3.0 derived through the integration of the Schechter parameters due to the high uncertainties in the derived parameters given the incompleteness at low masses. In the plots we also show a coloured area representing the upper and lower limits of the quiescent (red) and star-forming plus intermediate (blue) populations, as well as various results from literature. Orange symbols represent the stellar

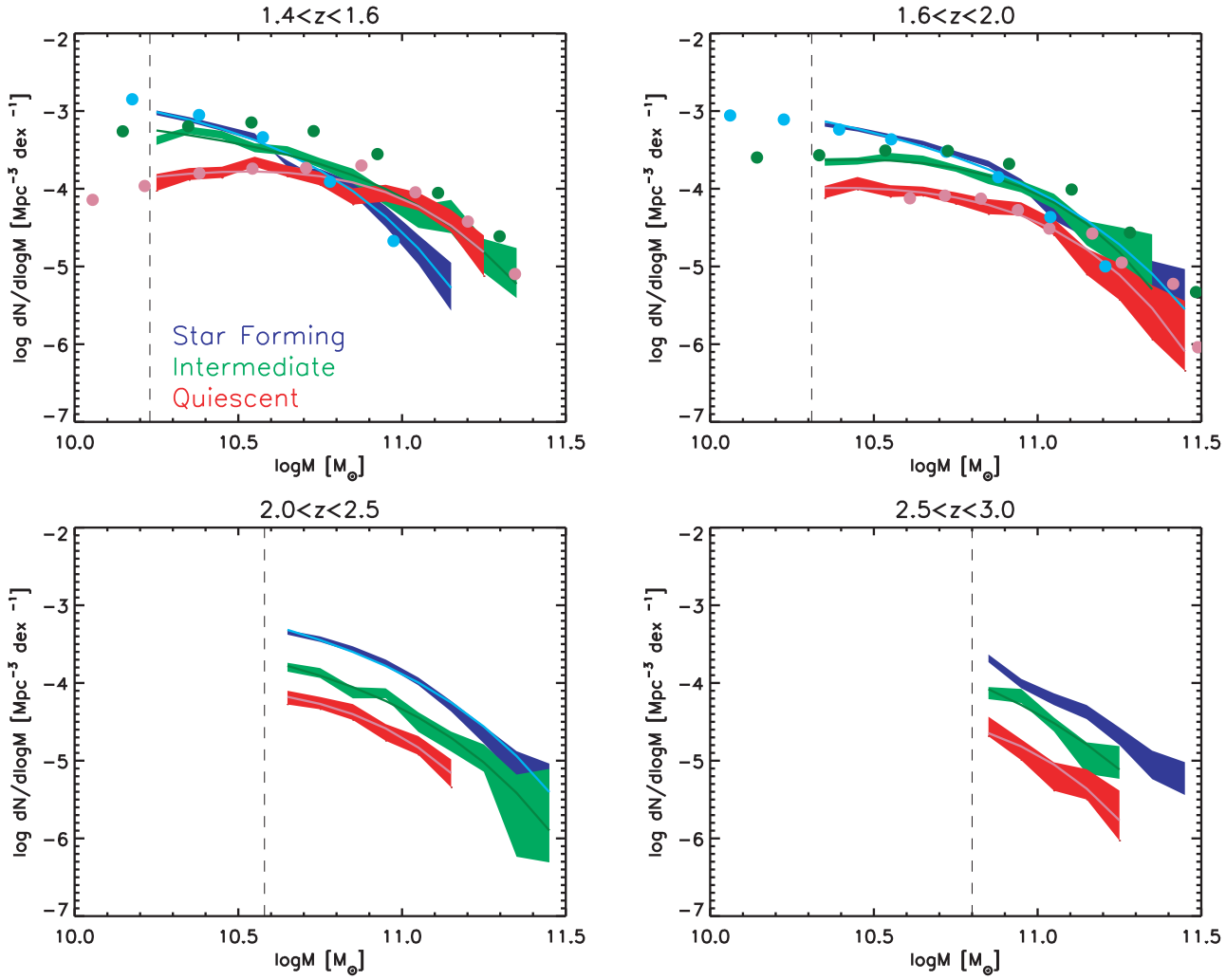

Figure 16. Evolution of the GSMF for different activity type galaxies. The coloured areas represent the upper and lower limits (see Section 7) while the thick lines are the Schechter fitting to the data. Red: quiescent. Green: intermediate. Blue: actively star forming. The circles represent the GSMF for quiescent (purple), intermediate (dark green) and high-activity galaxies (light blue), as obtained by Ilbert et al. (2010). Also shown are the limits in mass (vertical dashed lines).

mass density of the quiescent galaxies as derived by other authors, while light blue symbols stand for the star-forming ones (squares from Kochanek et al. 2001, diamonds from Driver et al. (2006), plus symbols from Bell et al. (2003), triangles from Arnouts et al. 2007, asterisks from Franceschini et al. 2006, crosses from Borch et al. (2006), dots from Ilbert et al. 2010). We are in very good agreement with Ilbert et al. (2010) in the common redshift bins. We observe that the increase in stellar mass density in the redshift range of interest ($t \sim 2$ to 4.5 Gyr) is very rapid for both populations (∼0.5 dex for the star-forming plus intermediate populations and ∼0.9 dex for the quiescent one), then slowing down at lower redshifts. However, this slow down happens earlier in time for the star-forming population ($z \sim 1.2$, $t \sim 5.0$ Gyr) than for the quiescent galaxies, which continue to rapidly assembly mass until later times ($z \sim 1.0$, $t \sim 6.0$ Gyr), reaching the star-forming galaxies mass density at $z < 1.0$.

The existence of a non negligible population ($\log \rho[\mathrm{M}_\odot\ \mathrm{Mpc}^{-3}] \sim 6.0$ at $z \sim 2.7$) of quiescent galaxies which have already undergone major star formation even at the highest redshifts ($z > 2.5$) is fundamental for our understanding of the galaxy formation processes and crucial for testing theoretical scenarios.

9 SUMMARY AND CONCLUSIONS

We derived the GSMF and stellar mass density in a 1.73 deg^2 area in the COSMOS field from $z = 1.4$ to 3.0 for the whole sample and for the sample divided into populations, paying special attention to the quiescent one. The GSMF estimate is based on ∼18 000 galaxies with $\mathrm{mag}_{3.6\,\mu\mathrm{m}}$ <22.0 and $z_\mathrm{p} \geq 1.4$. We summarize our results below.

(i) We find that an IRAC selected sample is fundamental for studying quiescent galaxies at high redshift. About 88 and 91 per cent of the K_s and IRAC subsamples are found at $z \gtrsim 1.4$ respectively, with this fraction dropping to 21 per cent for an i^+-band selected sample. Considering the galaxy classification, 62 per cent of the optically selected subsample is fitted by a blue template, while the same fraction is much lower (∼7 per cent) for the IRAC subsample.

(ii) We study the main properties of the high redshift quiescent sample ($z \geq 1.4$), finding that they are old and massive galaxies, with $\langle M \rangle \sim 10^{10.65}\ \mathrm{M}_\odot$ and ages ranging from ∼1 to ∼4 Gyr. They have small e-folding time-scales $\tau \sim 0.1$–0.3 Gyr and very low

Table 5. Schechter parameters of the QSMF at $1.4 \leq z \leq 3.0$.

Type	z-bin	α	$\log(M^*)(M_\odot)$	$\phi(10^{-4}\,\mathrm{Mpc}^{-3}\,\mathrm{dex}^{-1})$
Quiescent	1.4–1.6	-0.08 ± 0.98	10.57 ± 0.25	1.9 ± 0.5
	1.6–2.0	-0.41 ± 0.92	10.61 ± 0.19	1.0 ± 0.4
	2.0–2.5	-0.34 ± 4.83	10.50 ± 0.84	0.9 ± 0.8
	2.5–3.0	-0.34 (fixed)	10.52 ± 0.18	0.5 ± 0.6

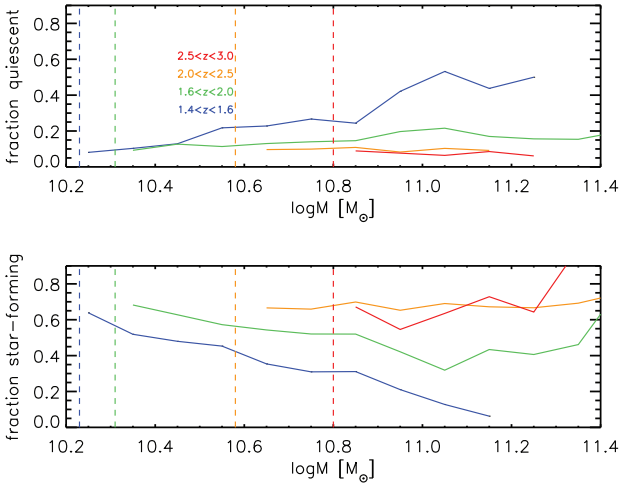

Figure 17. Upper panel: fraction of quiescent galaxies over total for different mass values. Colours represent the different redshift bins as in Fig. 15. Lower panel: fraction of the star-forming population over total versus mass. Coloured vertical dashed lines are the mass limits for each redshift bin.

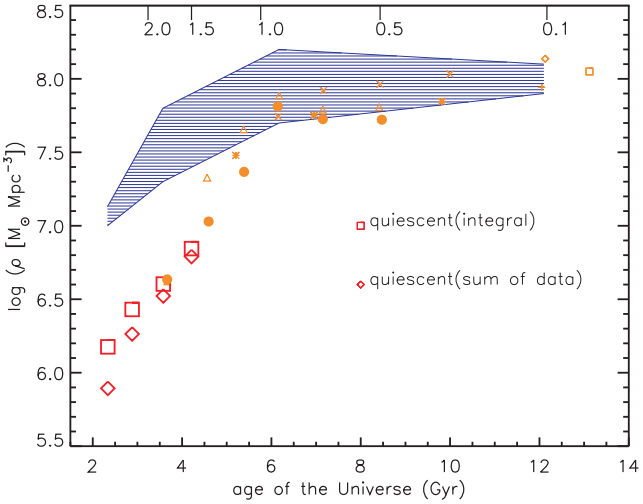

Figure 19. Evolution of the stellar mass density of quiescent galaxies. The result from this work are the red symbols. The values represented by the squares have been calculated as the integral of the Schechter function fitting the data, while the diamonds are a mere sum of the data for all masses. Orange symbols are results from literature as explained in the article. We also show for comparison the evolution of the stellar mass density of the star-forming plus the intermediate galaxies (blue shaded area).

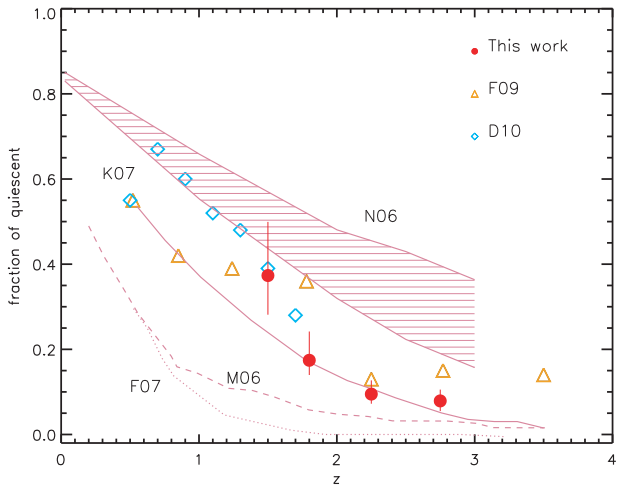

Figure 18. Fraction of quiescent galaxies ($\log(\mathrm{SSFR}[\mathrm{Gyr}^{-1}]) < -2$) with $M \geq 10^{10.85}\,M_\odot$ as a function of redshift. Red circles are the results obtained in this work (errors are the combination of the Poisson errors and the Monte Carlo simulations), orange triangles are the values from Fontana et al. (2009) and light blue diamonds from Damen et al. (2011). Lines refer to the predictions of theoretical models as described in the legend: Menci et al. (2006) (M06), Kitzbichler & White (2007) (K07), Nagamine et al. (2006) (N06) and Fontanot et al. (2007) (F07).

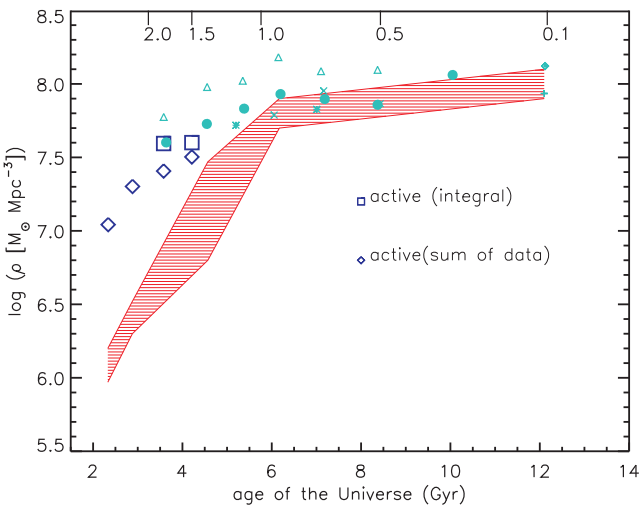

Figure 20. Evolution of the stellar mass density of star-forming plus intermediate galaxies. The result from this work are the dark blue symbols. The values represented by the squares have been calculated as the integral of the Schechter function fitting the data, while the diamonds are a mere sum of the data for all masses. Light blue symbols are results from literature as explained in the article. We also show for comparison the evolution of the stellar mass density of the quiescent galaxies (red shaded area).

dust extinction ($E(B-V) \sim$0–0.15), meaning passively evolving populations.

(iii) We observe a significant evolution of the QSMF from $2.5 < z < 3.0$ to $1.4 < z < 1.6$, amounting to $\sim$1 dex for galaxies with $\log M \sim 11.0$. The evolution is $\sim$0.3 dex in each redshift bin, meaning that the number of quiescent galaxies continuously increases with cosmic time.

(iv) We find that $z \sim 1.5$ is a clear epoch of transition of the GSMF: while the GSMF at $z \gtrsim 1.5$ is dominated by the star-forming galaxies at all stellar masses, at $z \lesssim 1.5$ the contribution to the total GSMF of the quiescent galaxies is significant and the quiescent galaxies become more important than the star-forming population for $M \geq 10^{10.75}\,\mathrm{M}_{\odot}$.

(v) The fraction of star-forming galaxies decreases from 60 to 20 per cent from $2.5 < z < 3.0$ to $1.4 < z < 1.6$ for $M \sim 10^{11.0}\,\mathrm{M}_{\odot}$, while the quiescent population increases from 10 to 50 per cent at the same z and mass intervals.

(vi) All of the theoretical models agree in predicting a gradual increase with cosmic time in the fraction of galaxies with a low SFR. However, only the K07 Millennium-based model is able to properly reproduce the shape of the data.

(vii) We find a significant number of quiescent galaxies already in place at $z > 2.5$ ($\log\rho\ [\mathrm{M}_{\odot}\,\mathrm{Mpc}^{-3}] \sim 6$), meaning that these galaxies assembled most of their stellar mass in previous epochs in an active starburst phase or through important merging processes at higher redshifts.

ACKNOWLEDGMENTS

This work was supported by an International grant from Instituto de Astrofísica de Canarias (IAC) with funding from the Research Structures Departments of Instituto Nazionale di Astrofísica (INAF). We thank the anonymous referee for the useful comments which helped to improve the original manuscript.

REFERENCES

Abraham R. G. et al., 2007, AJ, 669, 184
Arnouts S. et al., 2001, A&A, 379, 740
Arnouts S. et al., 2007, A&A, 476, 137
Baldry I. K., Glazebrook K., Brinkmann J., Ivezič Z., Lupton R. H., Nichol R. C., Szalay A. S., 2004, ApJ, 600, 681
Bell E. F., McIntosh D. H., Katz N., Weinberg M. D., 2003, ApJS, 149, 289
Bell E. F. et al., 2004, ApJ, 608, 752
Bolzonella M. et al., 2010, A&A, 524, 76
Borch A. et al., 2006, A&A, 453, 869
Brinchmann J., Charlot S., White S. D. M., Tremonti C., Kauffmann G., Heckman T., Brinkmann J., 2004, MNRAS, 351, 1151
Brown M. J. I., Dey A., Jannuzi B. T., Brand K., Benson A. J., Brodwin M., Croton D. J., Eisenhardt P. R., 2007, ApJ, 654, 858
Bruzual G., Charlot S., 2003, MNRAS, 344, 1000
Bundy K., Ellis R. S., Conselice C. J., Cooper M., Weiner B., Taylor J., Willmer C., 2005, BAAS, 37, 11235
Calzetti D., Armus L., Bohlin R. C., Kinney A. L., Koornneef J., Storchi-Bergmann T., 2000, ApJ, 533, 682
Capak P. et al., 2007, ApJS, 172, 99
Caputi K. I., Cirasuolo M., Dunlop J. S., McLure R. J., Farrah D., Almaini O., 2011, MNRAS, 413, 162
Cassata P. et al., 2008, A&A, 483, L39
Chabrier G., 2003, PASP, 115, 763
Ciliegi P., Zamorani G., Hasinger G., Lehmann I., Szokoly G., Wilson G., 2003, VizieR Online Data Catalog, 339, 80901
Cimatti A., 2006, Nuovo Cimento B Serie, 121, 1383
Cimatti A., 2009, in Giobbi G., Tornambe A., Raimondo G., Limongi M., Antonelli L. A., Menci N., Brocato E., eds, AIP Conf. Ser. Vol. 1111, The Formation and Evolution of Early-type Galaxies: Solid Results and Open Questions. Am. Inst. Phys., New York, p. 191
Cimatti A. et al., 2004, Nat, 430, 184
Cimatti A. et al., 2008, A&A, 482, 21
Cirasuolo M., McLure R. J., Dunlop J. S., 2007, Nuovo Cimento B Serie, 122, 1133
Cole S., Norberg P., Baugh C. M., Frenk C. S., Bland-Hawthorn E., 2001, MNRAS, 326, 255
Cowie L. L., Songaila A., Hu E. M., Cohen J. G., 1996, AJ, 112, 839
Daddi E., Cimatti A., Renzini A., Fontana A., Mignoli M., Pozzetti L., Tozzi P., Zamorani G., 2004, ApJ, 617, 746
Damen M. et al., 2011, ApJ, 727, 1
Dickinson M., Papovich C., Ferguson H. C., Budavári T., 2003, ApJ, 587, 25
Driver S. P. et al., 2006, MNRAS, 368, 414
Faber S. M. et al., 2007, ApJ, 665, 265 (F07)
Fontana A. et al., 2006, A&A, 459, 745
Fontana A. et al., 2009, A&A, 501, 15
Fontanot F., Monaco P., Silva L., Grazian A., 2007, MNRAS, 382, 903
Franceschini A. et al., 2006, A&A, 453, 397
Franx M. et al., 2003, ApJ, 587, L79
Franx M., van Dokkum P. G., Schreiber N. M. F., Wuyts S., Labbé I., Toft S., 2008, ApJ, 688, 770
Gallazzi A., Charlot S., Brinchmann J., White S. D. M., 2006, MNRAS, 370, 1106
Giallongo E., Salimbeni S., Menci N., Zamorani G., Fontana A., Dickinson M., Cristiani S., Pozzetti L., 2005, ApJ, 622, 116
Ilbert O. et al., 2006, A&A, 457, 841
Ilbert O. et al., 2009, ApJ, 690, 1236
Ilbert O. et al., 2010, ApJ, 709, 644
Kitzbichler M. G., White S. D. M., 2007, MNRAS, 376, 2 (K07)
Kochanek C. S. et al., 2001, ApJ, 560, 566
Kriek M. et al., 2008, ApJ, 677, 219
Kriek M. et al., 2010, ApJ, 722, L64
Le Floc'h E. et al., 2009, ApJ, 703, 222
Lilly S. J., Le Fevre O., Hammer F., Crampton D., 1996, ApJ, 460, L1
Lilly S. J., Le Fèvre O., Renzini A., Zamorani G., Scodeggio E., 2007, ApJS, 172, 70
Lilly S. J., Le Brun V., Maier C., Mainieri V., Mignoli M., Scodeggio M., Zamorani E., 2009, ApJS, 184, 218
McCarthy P. J., 2004, BAAS, 36, 128.06
McCracken H. J., Capak P., Salvato M., Aussel H., Thompson D., Daddi E., 2010, ApJ, 708, 202
Madau P., Ferguson H. C., Dickinson M. E., Giavalisco M., Steidel C. C., Fruchter A., 1996, MNRAS, 283, 1388
Mancini C., Matute I., Cimatti A., Daddi E., Dickinson M., Rodighiero G., Bolzonella M., Pozzetti L., 2009, A&A, 500, 705
Maraston C., 2005, MNRAS, 362, 799
Marchesini D., van Dokkum P. G., Förster Schreiber N. M., Franx M., Labbé I., Wuyts S., 2009, ApJ, 701, 1765
Marchesini D. et al., 2010, ApJ, 725, 1277
Menci N., Fontana A., Giallongo E., Grazian A., Salimbeni S., 2006, ApJ, 647, 753 (M06)
Mobasher B., Dickinson M., Mobasher B., Ferguson H. C., Giavalisco M., Wiklind T., 2004, BAAS, 37, 178.08
Nagamine K., Ostriker J. P., Fukugita M., Cen R., 2006, ApJ, 653, 881 (N06)
Nichol R. C., Cannon R., Roseboom I., Wake D., 2007, Heating versus Cooling in Galaxies and Clusters of Galaxies. Springer, Verlag, p. 422
Nicol M.-H., Meisenheimer K., Wolf C., Tapken C., 2011, ApJ, 727, 51
Pannella M., Hopp U., Saglia R. P., Bender R., Drory N., Salvato M., Gabasch A., Feulner G., 2006, ApJ, 639, L1
Pérez-González P. G. et al., 2008, ApJ, 675, 234
Polletta M. et al., 2007, ApJ, 663, 81
Pozzetti L., Madau P., Zamorani G., Ferguson H. C., Bruzual A. G., 1998, MNRAS, 298, 1133
Pozzetti L. et al., 2010, A&A, 523, A13

Prevot M. L., Lequeux J., Prevot L., Maurice E., Rocca-Volmerange B., 1984, A&A, 132, 389
Renzini A., 2006, ARA&A, 44, 141
Rodighiero G., Cimatti A., Franceschini A., Brusa M., Fritz J., Bolzonella M., 2007, A&A, 470, 21
Sanders D. B. et al., 2007, ApJS, 172, 86
Schechter P., 1976, ApJ, 203, 297
Schmidt M., 1968, ApJ, 151, 393
Scoville N. et al., 2007, ApJS, 172, 1
Somerville R. S., Lee K., Ferguson H. C., Gardner J. P., Moustakas L. A., Giavalisco M., 2004, ApJ, 600, L171
Sutherland W., Saunders W., 1992, MNRAS, 259, 413
Taylor E. N. et al., 2009, ApJ, 694, 1171
van Dokkum P. G. et al., 2010, ApJ, 709, 1018
Willmer C. N. A. et al., 2006, ApJ, 647, 853
Yan L., McCarthy P. J., Weymann R. J., Malkan M. A., Teplitz H. I., Storrie-Lombardi L. J., Smith M., Dressler A., 2000, AJ, 120, 575
Yan H., Dickinson M., Giavalisco M., Stern D., Eisenhardt P. R. M., Ferguson H. C., 2006, ApJ, 651, 24
Zucca E. et al., 1997, A&A, 326, 477

This paper has been typeset from a TEX/LATEX file prepared by the author.